A pH-Induced Dissociation of the Dimeric Form of a Lysine 49-Phospholipase A_2 Abolishes Ca^{2+}-Independent Membrane Damaging Activity†

A. H. C. de Oliveira,‡ J. R. Giglio,‡ S. H. Andrião-Escarso,‡ A. S. Ito,§ and R. J. Ward*,‖

Department of Chemistry, FFCLRP-USP, Department of Biochemistry and Immunology, FMRP-USP, and Department of Physics and Mathematics, FFCLRP-USP, Universidade de São Paulo, Ribeirão Preto-SP, Brazil

Received November 21, 2000; Revised Manuscript Received April 4, 2001

ABSTRACT: The hydrolysis of phospholipids by class II phospholipase A_2 (PLA_2) involves a Ca^{2+} ion cofactor bound to the Asp49 residue in the active site region. In the lysine 49 phospholipase A_2 homologues (Lys49-PLA_2), the Asp49 residue is substituted by Lys, and consequently the Lys49-PLA_2s show no Ca^{2+} binding and no detectable phospholipid hydrolysis. Nevertheless, the Lys49-PLA_2s demonstrate membrane damaging activity by an incompletely understood Ca^{2+}-independent mechanism of action. Using a combination of steady-state and time-resolved fluorescence techniques, we have examined the effect of pH on the monomer−dimer equilibrium of bothropstoxin I (BthTX-I), a Lys49-PLA_2 from the venom of *Bothrops jararacussu* which contains a single Trp77 residue located at the dimer interface. At pH 5.0, we observe a decreased quantum yield, a decreased rotational correlation time, and an increased bimolecular quenching rate constant with iodide. These results are consistent with a pH-induced dissociation of the BthTX-I dimer, with the consequent exposure of the Trp77 residue to aqueous solvent. In the presence of liposomes, membrane damaging activity is observed only under conditions in which the dimeric form of the BthTX-I is favored. These results demonstrate that the dimeric form of the protein is essential for the initiation of the Ca^{2+}-independent membrane damaging activity.

Phospholipases A_2 (PLA_2,[1] EC 3.1.1.4, phosphatide *sn*-2 acylhydrolases) hydrolyze the *sn*-2 ester bonds of *sn*-3 phospholipids, generating free fatty acids and lysophospholipids as reaction products (*1*). On the basis of amino acid sequence similarity, disulfide bond patterns, tissue specificity, and cellular function, the PLA_2s are currently classified into 10 groups (*2*). Groups I and II are structurally related secretory PLA_2s with molecular weights of 13−16 kDa, which are widely distributed and are particularly abundant in pancreatic secretions and snake venoms (*3*, *4*).

The hydrolysis of phospholipids by group I and II PLA_2s involves a highly conserved His48/Asp99 doublet in the catalytic site together with a conserved water molecule, which acts as the nucleophile in the catalytic mechanism. A Ca^{2+} ion cofactor which is bound by the carboxyl oxygen atoms of Asp49 and the carbonyl main chain oxygens of the neighboring calcium binding loop stabilizes the tetrahedral intermediate during catalysis. (*5*, *6*). Site-directed mutagenesis studies have demonstrated that substitution of Asp49 by Lys effectively eliminates binding of the Ca^{2+} cofactor (*7*), with a concomitant loss of catalytic activity (*8*). A subfamily of group II PLA_2s has been described in which Asp49 is substituted by Lys (*9*), and the crystal structures of several Lys49-PLA_2s have demonstrated that the ϵ-amino group of Lys49 is located in the position occupied by Ca^{2+} in the Asp49-PLA_2s (*10*−*12*). These Lys49-PLA_2s demonstrate no detectable hydrolytic activity, and it has been suggested that the Asp49Lys substitution eliminates productive binding of the Ca^{2+} cofactor with the consequent loss of catalytic function (*13*, *14*). Recent independent crystallographic data from two Lys49-PLA_2s have demonstrated the presence of a fatty acid molecule in the substrate binding cleft of the protein, which has led to the suggestion that although the Lys49-PLA_2s may support phospholipid hydrolysis, they fail to release the fatty acyl product resulting in an interrupted catalytic cycle (*15*, *16*). Nevertheless, despite the possibility of an interrupted catalytic cycle and the lack of measurable hydrolytic activity, the Lys49-PLA_2s retain a Ca^{2+}-independent membrane damaging activity (*17*−*19*).

Bothropstoxin I (BthTX-I) is a Lys49-PLA_2 isolated from the venom of *Bothrops jararacussu* (*20*), which forms homodimers in solution (*21*). The crystal structures of BthTX-I reveal that reciprocal contacts between the N-terminal helices and the tips of the short β-sheets in partner molecules stabilize the dimeric form of the protein. Furthermore, reorientation of the β-turn at the apex of the β-sheet together with an increased twist in the flanking β-strands imparts conformational flexibility which permits the interface

† This work was supported by FAPESP [Grants 96/11165-3 (R.J.W.), 97/14370-0 (A.H.C.O.), and 96/12492-8 (ASI)] and CNPq [Grants 300725/98-1 (R.J.W.) and 300816/94-4 (A.S.I.)].

* Corresponding author. Tel: (++55) (0)16 6024384. Fax: (++55) (0)16 6338151. E-mail: rjward@fmrp.usp.br.

‡ Department of Biochemistry and Immunology.

§ Department of Physics and Mathematics.

‖ Department of Chemistry.

[1] Abbreviations: PLA_2, phospholipase A_2; Asp49-PLA_2, phospholipase A_2 with an aspartic acid at position 49; Lys49-PLA_2, phospholipase A_2 homologue with a lysine at position 49; BthTX-I, bothropstoxin I, Lys49-PLA_2 from *Bothrops jararacussu* venom; ITFE, intrinsic tryptophan fluorescence emission; BS^3, bis(sulfosuccinimidyl) suberate; EYPC, egg yolk phosphatidylcholine (egg yolk lecithin); DMPA, dimyristoylphosphatidic acid.

10.1021/bi0026728 CCC: $20.00
Published on Web 05/18/2001

region to function as a molecular hinge (*21*). These observations led to a model for the Ca^{2+}-independent membrane damaging activity in which it was proposed that a quaternary conformation transition of the membrane-associated BthTX-I dimer results in significant relative movement of the two monomers leading to perturbation of the associated lipid molecules and the consequent disruption of the bilayer (*21*). The presence of a dimer is clearly crucial for the validity of this hypothesis, and we here present results which demonstrate that reduced pH causes the dissociation of the dimeric form of BthTX-I in solution. Furthermore, Ca^{2+}-independent membrane damaging activity is observed only under those conditions where dimers are observed in solution. These results lead us to suggest that the dimeric form of BthTX-I is essential to initiate the Ca^{2+}-independent membrane damaging mechanism.

MATERIALS AND METHODS

Protein Purification and Sample Preparation. Bothropstoxin I (BthTX-I) from desiccated *B. jararacussu* whole venom was purified by a single step cation-exchange chromatography protocol as described previously (*20*) and stored lyophilized at −20 °C until further use. Stock solutions of the lyophilized protein were prepared at a final concentration of 440 μM and centrifuged at 12000*g* for 5 min. The molecular weight of the BthTX-I monomer calculated from the amino acid sequence was assumed to be 13 675 (*22*). The protein was diluted over a concentration range of 0.44−10 μM with a 20 mM phosphate/citrate buffer containing 150 mM NaCl at pH values between 5.0 and 7.5 (buffer A).

Steady-State Fluorescence Spectroscopy. Intrinsic tryptophan fluorescence emission (ITFE) spectra were measured between 300 and 450 nm with a SLM 8100 spectrofluorometer (Spectronic Instruments, Urbana, IL), using an excitation wavelength of 295 nm and 1 cm optical path-length quartz cuvettes. Both the excitation and emission slit widths were set to 8 nm, with a photomultiplier voltage of 650 V. Measurements were performed at 25 °C, and all protein emission spectra were corrected by subtraction of buffer blanks. The quantum yield of the intrinsic tryptophan emission of BthTX-I at pH 7.0 was assumed to be 0.14 (*21*).

Intrinsic tryptophan emission quenching by iodide was measured by incremental substitution of the NaCl in buffer A by NaI:buffer B (same as buffer A, except that NaCl was exchanged for 150 mM NaI). This ensured that any mixture of buffers A and B maintained the ionic strength constant throughout the experiment. In all quenching experiments with iodide, $Na_2S_2O_3$ was added to a final concentration of 100 μM to prevent the accumulation of I_3^-. ITFE spectra were integrated between 310 and 450 nm, and after subtraction of buffer blank spectra, the quenching was calculated using the Stern−Volmer equation:

$$F_0/F = 1 + K_{SV}[Q] \quad (1)$$

where F and F_0 are the integrated fluorescence emission intensities in the presence and absence of increasing quencher concentration, [Q]. Stern−Volmer quenching coefficients (K_{SV}) were derived by linear fitting of the [I^-] vs F_0/F data.

Steady-state intrinsic tryptophan emission anisotropy measurements were performed at a protein concentration of 4.4 μM using Glan-Thompson quartz excitation and emission polarizers with a SLM 8100 spectrofluorometer operating in "T-format". The fluorescence intensities of the vertical and horizontal emission components on excitation with vertically polarized light (I_{vv} and I_{vh}) were measured with a monochromator at a fixed emission wavelength of 350 nm and a 320 nm transmission filter (Schott WG320), respectively. The anisotropy signals from buffer blanks were subtracted, and the polarization (P) of the emission was calculated using

$$P = (I_{vv} - GI_{vh})/(I_{vv} + GI_{vh}) \quad (2)$$

where G was a machine-dependent correction factor measured with horizontally polarized excitation. From this value of P, the emission anisotropy, $\langle r \rangle$, was calculated according to

$$\langle r \rangle = 2P/(3 - P) \quad (3)$$

Time-Resolved Fluorescence. BthTX-I was diluted to a final concentration of 8.8 μM in buffer A at either pH 5.0 or pH 7.0, and the fluorescence lifetime and anisotropy decays were measured by the time-correlated single-photon counting technique. The Ti:sapphire laser (Tsunami, Spectra Physics) was tuned to give output with a selected wavelength of 885 or 900 nm, and a third harmonic generator BBO crystal (GWN-23PL, Spectra Physics) gave the 295 or 300 nm excitation pulse that was directed to an Edinburgh FL900 spectrometer (Edinburgh Instruments, U.K.). The IRF was typically 48 ps, and the time resolution was 6.0 ps per channel. The fluorescence intensity decay data were fitted with the multiexponential decay function:

$$I(t) = I_0 \sum_i^n \alpha_i e^{-t/\tau_i} \quad (4)$$

where the relative amplitudes, α_i, and the decay constants, τ_i, represent the numerical parameters recovered from the fitting algorithm provided by Edinburgh Instruments. The fractional intensities, f_i, are equal to

$$f_i = \alpha_i \tau_i / \sum \alpha_i \tau_i \quad (5)$$

Time-resolved anisotropy decays were calculated from $I_{vv}(t)$ and $I_{vh}(t)$ components collected consecutively over 1 min periods using a Glan-Thompson emission polarizer oriented either horizontally or vertically. Data were corrected by a G factor calculated from $I_{hv}(t)$ and $I_{hh}(t)$ components collected by alternating the Glan-Thompson emission polarizer and using a Soleil-Babinet compensator to provide horizontally polarized light. Five repetitions of the data collection cycle were performed, and the sum of the intensity decays was used to calculate the anisotropy decay, $r(t)$, as follows:

$$r(t) = (I_{vv}(t) - GI_{vh}(t))/(I_{vv}(t) + 2GI_{vh}(t)) \quad (6)$$

The anisotropy decay data were analyzed over a time scale of 0.15−10 ns using exponential fitting as follows:

$$r(t) = r_0 \sum_i^n \beta_i e^{-t/\phi_i} \quad (7)$$

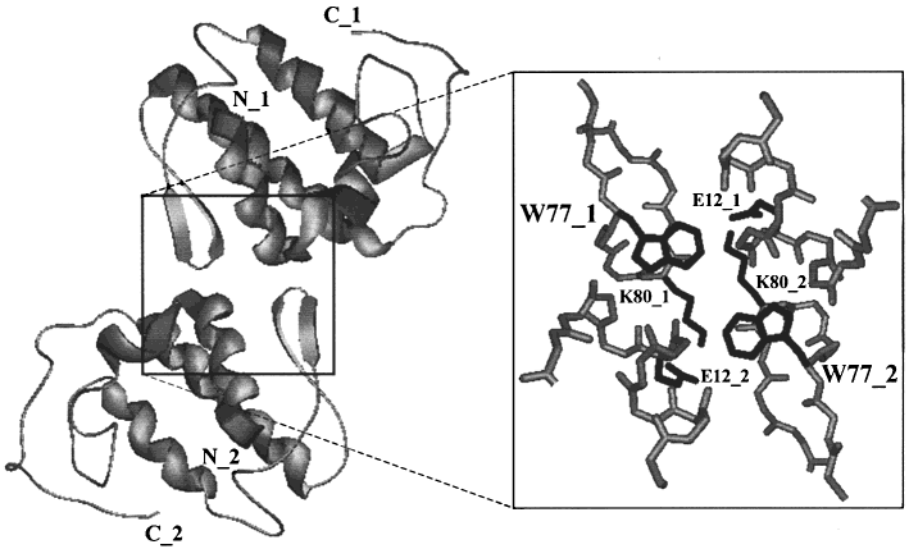

FIGURE 1: Ribbon representation of the crystal structure of the BthTX-I dimer (N and C termini of each monomer indicated) together with an expanded detail of the dimer interface region showing the residues E12, W77, and K80 from each monomer. Each BthTX-I monomer contains a single W77 residue, which is situated close to the 2-fold rotation axis of the dimer. Consequently, the two tryptophan residues are separated by a distance of ~8 Å in the dimeric form of the protein.

where β_i and ϕ_i were the recovered numerical parameters of the preexponential depolarization and correlation times which provided the best fit to the $r(t)$ function with the general constraint of r_0 equal to 0.3. For both the intensity and anisotropy decays, the adequacy of the exponential decay fitting was assessed by inspection of the plots of weighted residuals and by statistical parameters, such as reduced χ^2.

Chemical Cross-Linking. Solutions of 2.2 μM BthTX-I in buffer A (pH range 5.0−7.0) were incubated in the presence of 300 μM bis(sulfosuccinimidyl) suberate (BS^3; Pierce, Rockfort, IL) for 15 min at 25 °C. The reaction was halted by addition of TRIS, pH 8.0, to a final concentration of 50 mM, and the mixture heated at 95 °C for 3 min in the presence of 4 mM SDS and 10 mM β-mercaptoethanol. Samples were applied to sodium dodecyl sulfate−polyacrylamide gel electrophoresis (SDS−PAGE; *23*) using 16% discontinuous gels and electrophoresed at 100 mA for 2 h with subsequent silver staining.

Release of the Entrapped Fluorescent Marker from Liposomes. A loss of membrane integrity results in dilution of the liposome entrapped self-quenching fluorescent dye calcein, with a consequent increase in the fluorescence signal (*18*). The lipids egg yolk phosphatidylcholine (EYPC; Fluka Chemie, Switzerland) and dimyristroylphosphatidic acid (DMPA; Avanti Polar Lipids, Alabaster, AL) were stored as stock solutions at 10 and 100 mg·mL^{-1}, respectively, at −70 °C in $CHCl_3$ for a period not exceeding 3 months. A mixture of lipids containing a 9:1 molar ratio of EYPC:DMPA was evaporated under a stream of nitrogen and lyophilized under vacuum for 3−4 h. The dried lipid was solubilized in 1−2 mL of diethyl ether, to which was added 0.5 volume of 25 mM calcein (Sigma Química, São Paulo, Brazil) in 150 mM NaCl, 1 mM EGTA, and 25 mM phosphate/citrate buffer at pH 5.0 or 7.0. The mixture was sonicated briefly to produce an emulsion, and liposomes were prepared by reverse-phase evaporation (*24*). Liposomes were subsequently filtered through 400 nm pore size polycarbonate filters (Costar, Cambridge, MA), and the calcein-loaded liposomes were separated from the free marker by size exclusion chromatography using a Sephadex G-50 resin (Amersham-Pharmacia, São Paulo, Brazil). After estimation of the final phospholipid concentration (*25*), the filtered liposomes were mixed with 0.6 μM BthTX-I to give a protein:lipid molar ratio of 1:200, and the calcein release kinetics were monitored by the fluorescence increase at λ_{em} = 520 nm with λ_{ex} = 480 nm using an SLM 8100 fluorometer. The fluorescence signal was expressed as a percentage of total dye liberation on addition of 5 mM Triton X-100 on completion of the kinetic experiment.

RESULTS

The crystal structure of BthTX-I has been previously determined (*21*), and Figure 1 shows a ribbon representation of the molecule in which a homodimer is stabilized by contacts between the tips of the short β-sheets and the N-terminal α-helices. Figure 1 shows further detail of the interface region in which residues Glu12, Lys80, and Trp77 are highlighted. A previous analysis of the dimer interface has revealed that salt bridges between Glu12 in one molecule and Lys80 in the partner molecule contribute to the intermolecular contacts which stabilize the dimer (*21*). BthTX-I contains a single Trp residue at position 77, which also participates in the intermolecular contacts by hydrogen bonding with the main chain carbonyl oxygens of the partner molecules and through hydrophobic contacts (*21*).

Although surrounded by the protein matrix and largely hidden from the solvent, the microenvironment of Trp77 is highly polar due to the proximity of hydrophilic residues at the dimer interface (*21*). Figure 2 presents the intrinsic tryptophan fluorescence emission (ITFE) spectrum of BthTX-I which shows a maximum emission wavelength (λ_{max}) of 344.5 nm at pH 7.0, which is similar to that previously reported (*21*). Figure 2 further shows that as the pH is reduced to pH 5.0, the λ_{max} decreases to 341.5 nm (Figure 2B) and that this shift is accompanied by a decrease in the tryptophan quantum yield from 0.14 to 0.09 (Figure 2C). Results of intrinsic fluorescence lifetime decay experiments are summarized in Table 1, which show that at both

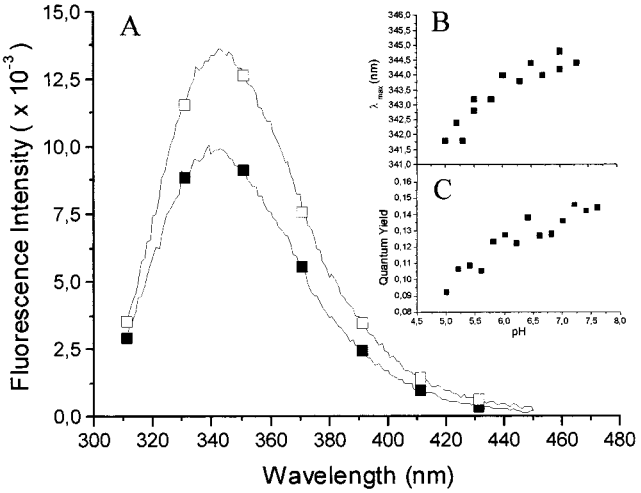

FIGURE 2: (A) Intrinsic tryptophan fluorescence emission spectra of BthTX-I at pH 5.0 (solid squares) and pH 7.0 (open squares) on excitation at 295 nm. (B) Effect of pH on the maximum emission wavelength (λ_{max}) of BthTX-I. (C) Effect of pH on the quantum yield of BthTX-I. In all experiments the protein concentration was 4.4 μM.

pH 7.0 and pH 5.0, the fluorescence decays were adequately described by the sum of three exponential functions. The calculated mean fluorescence lifetime at pH 7.0 was 3.2 ns as compared to 2.5 ns at pH 5.0, and this shorter mean fluorescent lifetime at pH 5.0 is consistent with the decreased quantum yield of BthTX-I observed at the same pH. These results demonstrate that a structural change occurs at reduced pH which results in an altered microenvironment of Trp77. However, the changes in the ITFE spectra are not accompanied by alteration in the far-ultraviolet (200−250 nm) circular dichrosim spectra, indicating that the secondary structure of BthTX-I remains intact at pH 5.0 (data not shown).

To investigate the nature of the structural change induced at lowered pH, quenching of the ITFE by iodide was measured over the pH range from 5.0 to 7.5. As shown in Figure 3A, at a protein concentration of 4.4 μM the Stern−Volmer quenching coefficient (K_{sv}) increases from 2.1 to 4.1 M^{-1} as the pH of the solution is reduced from pH 7.0 to pH 5.0. The dynamic quenching of tryptophan by iodide requires collision between the two species, and the bimolecular quenching rate constant (k_q) of this interaction is a sensitive probe for the solvent accessibility of tryptophan residues (*26*). Using the K_{SV} values of 4.1 and 2.0 measured at a protein concentration of 8.8 μM (Figure 3B) and weighted average lifetimes of 2.5 and 3.2 ns at pH 5.0 and 7.0, respectively (see Table 1), k_q values of 1.6×10^9 $M^{-1}\cdot s^{-1}$ at pH 5.0 and 0.6×10^9 $M^{-1}\cdot s^{-1}$ at pH 7.0 were observed. The increased

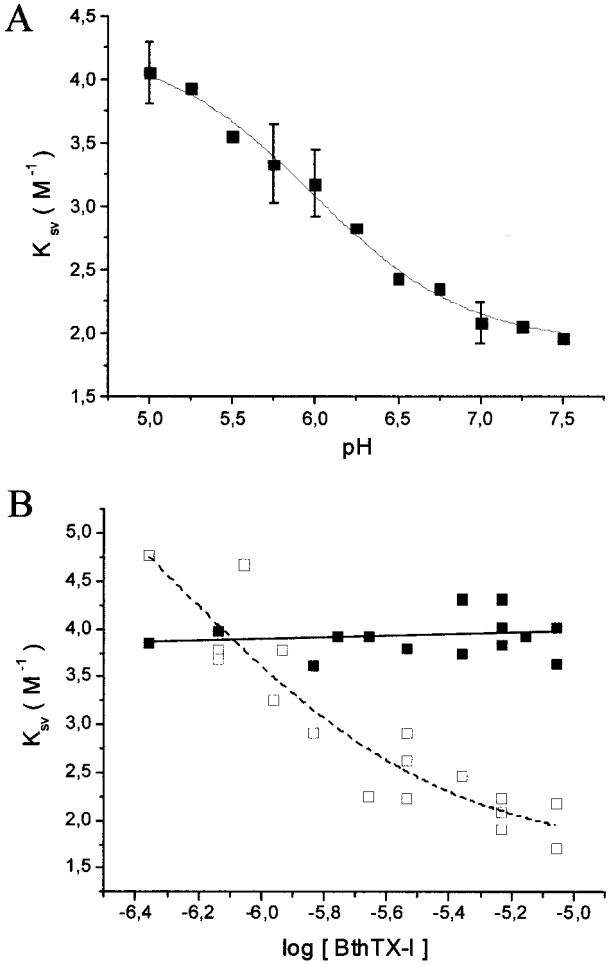

FIGURE 3: (A) Effect of pH on the Stern−Volmer constant (K_{SV}) for quenching of the intrinsic tryptophan fluoresence emission of BthTX-I by iodide at a protein concentration of 4.4 μM. The solid line represents the sigmoidal curve calculated by nonlinear regression analysis. (B) Effect of protein concentration on the Stern−Volmer constant (K_{SV}) for quenching of BthTX-I by iodide at pH 7.0 (open squares) and pH 5.0 (closed squares). The protein concentration range was varied between 0.44 and 8.8 μM.

k_q at pH 5.0 demonstrates that the Trp77 residue in BthTX-I becomes more solvent exposed at the lower pH. These data are consistent with the pH-induced dissociation of the BthTX-I dimer, and a sigmoid curve fit to the data in Figure 3A yields a midpoint pH value of 5.95. The pK_a values of acidic residues in apolar environments will be shifted to higher pH, and this result is consistent with the partial burial of the Glu12 residue at the dimer interface (see Figure 1).

The dimeric form of the protein occludes access of the quencher to Trp77 (*21*), and an increased solvent accessibility of this residue would be predicted on dissociation of the

Table 1: Fluorescence and Anisotropy Decay Parameters of BthTX-I in Buffer A at pH 7 and 5 with λ_{ex} = 300 nm[a]

	fluorescence intensity decay[c]								anisotropy decay[d]						
	lifetime (ns)			fractional intensity				mean lifetime	RCT[b] (ns)			preexponential value			
pH	τ_1	τ_2	τ_3	f_1	f_2	f_3	χ^2	(ns)	ϕ_1	ϕ_2	ϕ_3	b_1	b_2	b_3	χ^2
7.0	4.6	2.1	0.39	0.48	0.45	0.07	1.002	3.2	15.4	2.5	0.11	0.09	0.08	0.13	0.999
5.0	3.7	1.9	0.35	0.40	0.51	0.09	1.004	2.5	6.8		0.10	0.17		0.13	0.998

[a] The protein concentration in all experiments was 8.8 μM. See Materials and Methods for further experimental details. [b] Rotational correlation time. [c] Intensity decay data were fitted with the multiexponential decay function $I(t) = I_0\sum\alpha_1 \exp(-t/\tau_i)$. The fractional intensities are equal to $f_i = \alpha_i\tau_i/\sum\alpha_i\tau_i$. [d] Anisotropy decay data were fitted with the multiexponential decay function $r(t) = r_0\sum b_i \exp(-t/\phi_i)$.

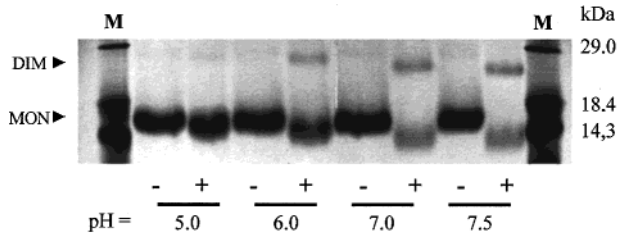

FIGURE 4: Silver-stained 16% PAGE−SDS gel showing the effect of pH on the chemical cross-linking of BthTX-I by BS^3 in solutions with pH values between 5.0 and 7.5. Lanes marked (+) are those incubations in the presence of BS^3, and lanes marked (−) are incubations in the absence of cross-linker. Monomer (MON) and dimer (DIM) bands are indicated. Lanes marked M are protein molecular weight markers, with molecular weights as indicated.

dimer. Although higher protein concentration favors dimer formation, dilution of BthTX-I should increase the fraction of the monomeric form, resulting in an increase in exposure of Trp77 to the solvent. Figure 3B demonstrates that at pH 7.0 an increase in the K_{SV} from 2.0 to 4.7 M^{-1} is observed as BthTX-I is diluted from 8.8 to 0.44 μM. Assuming that the increased K_{SV} is due to dissociation of the dimer, a self-association constant of 5×10^{-7} for BthTX-I at pH 7.0 was estimated. In contrast, at pH 5.0 a constant K_{SV} value of ~4.0 M^{-1} was observed over a similar protein concentration range. The slight increase in K_{SV} values observed in the diluted protein at pH 7.0 relative to pH 5.0 suggests a modest increase in the solvent accessibility of Trp77 in the monomeric forms between pH 7.0 and pH 5.0. However, it may be expected that significant tertiary structure changes would alter the circular dichrosim spectra in the near-ultraviolet (250−300 nm) region, and no differences were observed between the near-ultraviolet spectra of BthTX-I at pH 5.0 and 7.0 (data not shown). This indicates that separation of the dimers has at most only a slight effect on the tertiary structure of BthTX-I.

These results support the suggestion that the dimeric form of the BthTX-I is favored at protein concentrations above 4.4 μM at pH 7.0 and further indicate that at pH 5.0 the monomeric form is present at concentrations up to 8.8 μM. Additional evidence for the pH-induced quaternary structure transition in BthTX-I was obtained from chemical cross-linking experiments using the bifunctional cross-linker bis-(sulfosuccinimidyl) suberate (BS^3). This bifunctional reagent may covalently link tertiary amine groups separated by up to 11.4 Å, permitting both intra- and intermolecular reactions between Lys and Arg residues. The SDS−PAGE gel presented in Figure 4 demonstrates that at a BthTX-I concentration of 2.2 μM the covalently linked dimeric form is present at pH 7.0, whereas at pH 5.0 only the monomeric form is observed. The presence of a monomer band at higher pH values may reflect the importance of positively charged residues in dimer stabilization, the modification of which would increase the fraction of the monomeric form.

The ITFE, quenching, and chemical cross-linking data indicate that variation of pH between 5.0 and 7.0 results in quaternary structural changes in BthTX-I. Valuable information concerning the local tryptophan mobility and the overall conformation change in the dimeric and monomeric forms of the protein at pH 7.0 and 5.0 may be obtained from time-resolved fluorescence anisotropy decay experiments. As shown in Table 1, the time-resolved anisotropy decays were heterogeneous, and adequate decay fits were obtained using a biexponential function at pH 5.0 and a triexponential function at pH 7.0. The motions of the tryptophan indole ring in proteins occur over a time range spanning several orders of magnitude, and correlation times derived from anisotropy decay experiments represent the average rotational diffusion over a given time scale (*27*). Fast correlation times are generally ascribed to torsional vibrations of the indole ring within a permitted conformer well (*28*), and since the short correlation times of 110 ps at pH 5.0 and 100 ps at pH 7.0 observed in BthTX-I are similar to values observed for tryptophan containing peptides (*29*), we tentatively assign these components to the local tryptophan motion. The slower anisotropy decay components arise from molecular tumbling, local polypeptide backbone motions, and torsional rotation of the indole rings (*28*). Therefore, the slower correlation times of 6.8 ns at pH 5.0 and 15.4 ns at pH 7.0 may be ascribed to the overall rotation of the whole macromolecule, which is related to the geometry and hydrated volume of the protein.

Theoretical values for the slow correlation times (ϕ_c) were calculated using the Stokes−Einstein equation:

$$\phi_c = M(\nu + \delta)\eta/RT \qquad (8)$$

where M is the molecular weight of BthTX-I, ν and δ are the specific volume and the hydration state of the protein, respectively, η is the viscosity in centipoise, R is the gas constant, and T is the absolute temperature. In the present calculation, the value of the specific protein volume was taken as 0.73 $cm^3 \cdot g^{-1}$, with the hydration state of $0.35 g_{H_2O}/g_{protein}$ (*30*). This calculation yields values of 6.0 and 12.0 ns for the monomeric and dimeric forms, respectively, which are slightly lower than the rotational correlation times observed for the slower components in the anisotropy decays at pH 5.0 and 7.0, respectively. A spherical protein geometry is implicit in the rotational correlation time calculation, and the observed deviations from the ideal situation may be due to the nonspherical geometry of the BthTX-I molecule. Indeed, the crystal structure of the BthTX-I monomer presents an overall flattened ellipsoidal geometry, and the relative orientation of the monomers in the dimeric form of the BthTX-I results in a more elongated structure. It has been previously demonstrated that, for proteins which present nonspherical geometry, complex anisotropy decay curves can be expected (*31*). Therefore, molecular rotation around the long axis of the BthTX-I dimer might result in intermediate correlation times and may contribute to the 2.5 ns component observed in the decay curves at pH 7.0.

On a structural basis, it might be expected that the quaternary transition of BthTX-I from a dimeric to the monomeric form together with an increased mobility of Trp77 in the monomeric form at low pH would result in a decrease in the steady-state anisotropy signal. However, as shown in the inset to Figure 5, a decrease in the pH results in an increase in the steady-state ITFE anisotropy from 0.10 at pH 7.0 to 0.11 at pH 5.0. This result suggests that an additional depolarizing process contributes to reduce the anisotropy signal of BthTX-I at pH 7.0, and further insights as to the nature of this process may be obtained from the steady-state anisotropy excitation spectra. As shown in the

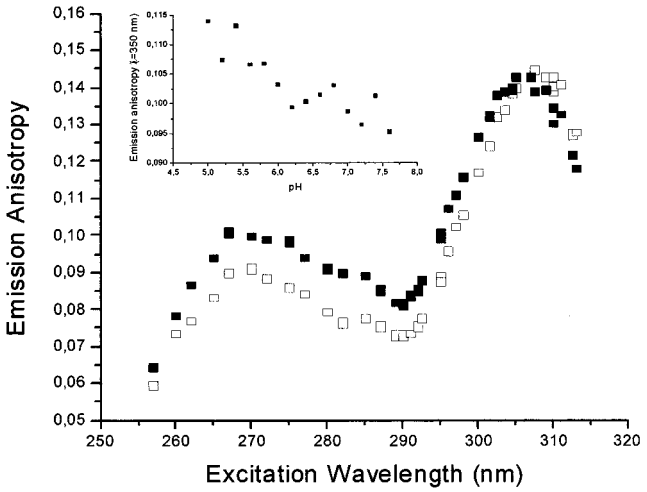

FIGURE 5: Steady-state anisotropy excitation spectra of BthTX-I at pH 5.0 (closed squares) and pH 7.0 (open squares). The inset demonstrates the effect of pH on the BthTX-I steady-state intrinsic tryptophan fluorescence anisotropy. The protein concentration in all experiments was 4.4 μM.

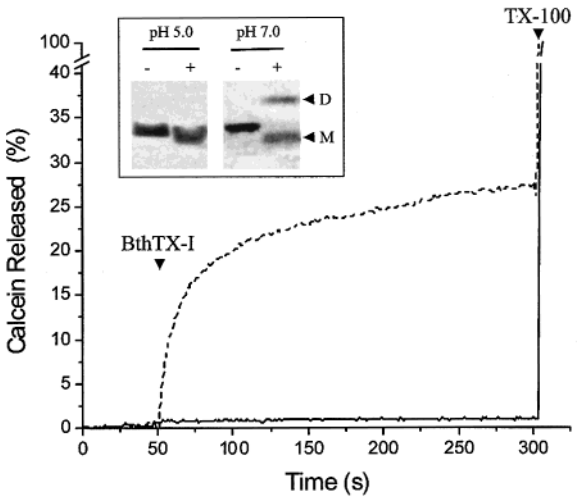

FIGURE 6: Release kinetics of the fluorescent marker calcein induced by BthTX-I from liposomes composed of a 9:1 molar ratio of egg yolk phosphotidylcholine (EYPC) and dimyristroylphosphatidic acid (DMPA) at pH 7.0 (dashed line) and pH 5.0 (solid line). The increase in the fluorescence signal on addition of BthTX-I (indicated on the figure) was monitored at $\lambda_{em} = 520$ nm with $\lambda_{ex} = 480$ nm and is presented as the percentage of total dye liberation after addition of 5 mM Triton X-100 (indicated by TX-100 on the figure). Inset: Silver-stained 16% PAGE−SDS gel showing the chemical cross-linking of BthTX-I by BS^3 in the presence of EYPC/DMPA liposomes at pH 5.0 and 7.0. Lanes (+) and (−) indicate in the presence or absence of BS^3 in the incubation. Monomer (M) and dimer (D) bands are indicated.

main panel of Figure 5, between excitation wavelengths of 257 and 305 nm the steady-state anisotropy values at pH 7.0 are lower than at pH 5.0, whereas above 305 nm the anisotropy values at pH 5.0 are less than at pH 7.0. Previous studies have demonstrated that changes in the steady-state anisotropy signal in the "red-edge" region of the tryptophan excitation spectra may arise due to resonance energy homotransfer between tryptophan molecules (*32*). In proteins, a homotransfer of energy between tryptophans is manifested as an increased steady-state anisotropy signal at 310 nm relative to that at 295 nm (r_{310}/r_{295}) (*33*). Figure 5 shows an increase in the r_{310}/r_{295} from 1.3 at pH 5.0 to 1.6 at pH 7.0, which supports the suggestion that resonance energy homotransfer occurs between Trp77 residues in the dimeric form of BthTX-I at pH 7.0.

Further evidence which is suggestive of a resonance energy homotransfer process at pH 7.0 may be derived from the time-resolved anisotropy results. The measured preexponential values of the anisotropy decays of Trps in rigid protein environments are in the range 0.2−0.22 (*34*, *35*). However, it has been reported that, in both LADH and interferon α_2, depolarization due to resonance energy homotransfer results in significantly reduced values for the preexponential terms of the slow anisotropy decay components (*36*, *37*). A resonance energy homotransfer process is therefore consistent with the preexponential value of 0.09 for the slow component of the anisotropy decay in the dimeric form of BthTX-I at pH 7.0. It is worthy of note that the anisotropy decays of Trp residues in more solvent exposed or less rigid environments have preexponential values of 0.16−0.17 (*34*, *35*), which is comparable with the preexponential term observed for the slow component of BthTX-I in the monomeric state at pH 5.0. The presence of a resonance energy homotransfer process between the Trp77 residues at the dimer interface at pH 7.0, and the absence of this process at pH 5.0, is in accord with a pH-induced transition between the monomeric and dimeric forms of the protein.

To evaluate the effect of the dimer to monomer transition on the Ca^{2+}-independent membrane damaging activity, disruption of liposome membranes by BthTX-I was assessed by measurement of the release kinetics of the liposome entrapped self-quenching fluorescent marker calcein at pH 5.0 and 7.0. In these experiments, damage to the liposome membrane results in the liberation from the liposomes and dilution of the self-quenching marker, with a consequent increase in the fluorescence emission. Figure 6 presents the release kinetics of the calcein from liposomes composed of EYPC and DMPA in a 9:1 molar ratio. At pH 7.0 the addition of BthTX-I results in a rapid liberation of the fluorescent marker with no detectable lag phase under the experimental conditions used. The inset to Figure 6 presents the results of chemical cross-linking of BthTX-I using BS^3 in the presence of liposomes of the same composition as used in the marker release experiments and which demonstrate that the dimeric form of the protein is maintained pH 7.0 in the presence of lipid membranes. In contrast, at pH 5.0 neither marker release nor the presence of dimers is observed, demonstrating that no membrane damaging activity is detected under conditions in which the monomeric form of the protein is favored.

DISCUSSION

Changes in the fluorescent properties of the single Trp77 in BthTX-I have previously been used to monitor conformation changes in the dimeric form of the protein at pH 7.0 (*21*). In the present paper we have combined steady-state and time-resolved fluorescence measurements together with biochemical techniques to evaluate the effect of pH on the quaternary structure of BthTX-I in solution. We have correlated these results with release studies of a liposome-entrapped marker, which suggests that the dimeric form of the protein is essential for the initiation of the membrane damaging process.

The crystal structures of Lys49-PLA_2s from several snake venoms have been solved in both the dimeric (*12*, *15*, *16*, *38*, *39*) and monomeric (*11*, *41*, *42*) forms. Analysis of the crystal structures of dimeric Lys49-PLA_2s reveals a pattern of reciprocal intermolecular interactions between the N-terminal helix and β-wing regions which involve residues Glu12, Trp77, and Lys80 (see Figure 1) (*12*, *15*, *16*, *39*, *42*). Salt-bridge formation between the carboxyl oxygens of Glu12 and the ϵ-amino group of Lys80 is a highly conserved feature of the homodimeric interaction. Furthermore, as a consequence of its localization at the dimer interface, Trp77 of BthTX-I is enclosed within the protein matrix and thereby shielded from the solvent in the dimeric form at pH 7.0 (*11*, *21*, *39*). The myotoxin I from *Bothrops godmani* has been observed as a monomer in the crystalline state, and on the basis of small-angle X-ray scatter results at pH 7.0 and 5.0, it has been suggested that the low pH crystallization conditions favored this form of the protein (*40*). Comparison of the dimeric form of BthTX-I crystallized at pH 7.0 with monomeric myotoxin I from *B. godmani* crystallized at pH 5.0 reveals that Trp77 becomes significantly more solvent exposed upon dissociation of the dimer. This change in solvent-exposed area in the crystal structures is consistent with the increased bimolecular quenching rate constant (k_q) observed with iodide at pH 5.0. Furthermore, the pH-dependent changes in the intrinsic tryptophan fluorescence emission, together with the absence of dimers in the chemical cross-linking and the reduced correlation times of the slow components in the time-resolved anisotropy experiments, are consistent with the dissociation of the BthTX-I dimer in solution at pH 5.0. The crystallographic and spectroscopic evidence indicates a high degree of structural similarity between the monomeric and dimeric forms of the protein, suggesting that structural changes are not responsible for the reduced dimer stability at lowered pH. The observed midpoint of the quaternary structure transition at pH 5.95 indicates that one or more acidic residues at the dimer interface participate in interactions which stabilize the dimer and suggests that electrostatic interactions play an important role in maintaining dimer stability.

The crystal structures of Lys49-PLA_2s in the monomeric form reveal that both the position of the Trp77 indole side chain and the conformation of the β-wing are only slightly altered in comparison to the dimeric Lys49-PLA_2s (*12*, *13*, *40*). We have observed that although Trp77 becomes more solvent exposed in the monomeric state at pH 5.0, the λ_{max} of the BthTX-I ITFE at this pH is slightly reduced in relation to that observed at pH 7.0 (Figure 2). This shift in the λ_{max} may be due to alterations in tertiary structure; however, the similarity of the dimeric and monomeric crystal forms of the Lys49-PLA2s, together with the absence of significant differences in the near-ultraviolet circular dichroism spectra at pH 5.0 and 7.0, suggests that the monomer separation has only a minor effect on the tertiary structure of BthTX-I. The ITFE λ_{max} may be further influenced by the red-edge excitation shift effect, in which an incomplete reorientation of immobile dipoles in the environment immediately surrounding a Trp indole ring leads to reduced electronic transition energies and a red shift of the ITFE spectrum (*43*, *44*). Although the λ_{ex} of 295 nm used in the steady-state experiments is below the limit where the red-edge effect is normally observed for Trp residues in proteins (*43*, *44*), Figure 5 demonstrates that at this wavelength resonance energy homotransfer occurs between adjacent Trp77 residues in the BthTX-I dimer at pH 7.0. We suggest that, in the dimeric form, those Trp residues excited at a λ_{ex} below the red edge in one molecule may act as donors for resonance energy homotransfer to an acceptor Trp located in the partner molecule of the dimer. Homotransfer will occur only if the excited state of the acceptor Trp is in a lower vibrational energy state than the donor; thus conditions are established for red-edge emission from the acceptor Trp. In the absence of homotransfer in the monomeric form of BthTX-I at pH 5.0, no red-edge effect would be observed at a λ_{ex} of 295 nm, and the measured λ_{max} would be reduced. This suggestion is supported by solution studies in which a small but nonetheless significant shift in the emission spectrum toward longer wavelengths was observed in aromatic fluorophores (including Trp) under conditions in which homotransfer is favored (*32*).

The pH-induced quaternary structure change of BthTX-I results in significant alterations in the time-resolved anisotropy decays of Trp77. The model employed in the anisotropy decay analysis assumes that fast and slow correlation times arise from independent motions of the tryptophan indole ring. However, as observed in other protein studies, an analysis assuming nonassociative anisotropy decay due to fast and slow movements of Trp residues may be an oversimplification (*34*, *35*). In the homodimer of horse LADH (lactic acid dehydrogenase), the Trp314 residues from each monomer are immobilized at the dimer interface with a separation of $\sim$7 Å between the indole rings. A rapid depolarization process involving these two residues which is consistent with resonance energy homotransfer has been observed in the time-resolved anisotropy decay (*34*). In human interferon α_2, the observed anisotropy decay could be successfully modeled by including a resonant energy homotransfer process between adjacent Trp residues buried within the protein matrix (*35*). We suggest that an additional contribution to the anisotropy decay of BthTX-I at pH 7.0 may arise from depolarization due to resonance energy homotransfer between the adjacent Trp77 residues at the dimer interface. The BthTX-I excitation anisotropy spectrum (Figure 5) suggests that, at an excitation wavelength of 300 nm, resonance energy homotransfer may provide a significant contribution to the steady-state anisotropy. In the BthTX-I crystal structure, the distance between the centers of mass of the Trp77 indole rings is approximately 8 Å. Calculation of the orientation factor based on the relative positions of the Trp77 indole side chains at the dimer interface, together with estimation of the overlap of isoenergetic states between the absorption and emission spectra, predicts a Forster radius value of $\sim$11 Å. These theoretical calculations indicate that resonance energy homotransfer in the dimeric state of BthTX-I is feasible and predict that the process may be efficient. The reduced preexponential values of the slow component of the anisotropy decay provide supportive evidence that the homotransfer process occurs at pH 7.0, and as would be expected on dissociation of the dimer, the process is absent at pH 5.0.

Previous studies have indicated that dimerization may play a functional role in the catalytically active Asp49-PLA_2s. The stability of the *Crotalus atrox* PLA_2 dimer is favored at

pH 7.0 (*45*, *46*), and kinetic studies of substrate hydrolysis of both this protein (*47*) and the closely related PLA$_2$ from *Crotalus adamanteus* (*48*) have indicated that the membrane active form is dimeric. Although these results were corroborated by chemical modification (*49*) and analytical centrifugation techniques (*50*), further investigation concluded that the active form might be either a monomer or a dimer (*46*). Nevertheless, the crystal structure of the PLA$_2$ from *C. atrox* presents a dimer conformation in which the substrate binding and catalytic sites are shielded by the dimer interface, and a quaternary structure transition of the membrane-bound enzyme has been proposed which would permit access of substrate and Ca^{2+} ions to these regions (*51*). Dimerization of Asp49-PLA$_2$s may also be associated with the increased catalytic activity observed on interaction with aggregated substrates. The lag phase of the catalytic activity observed with the Asp49-PLA$_2$ from *Agkistrodon piscivorus piscivorus* has been suggested to be the consequence of a membrane-dependent transition between monomeric and dimeric forms of the membrane-associated protein (*52*, *53*). It should be noted that structural changes in these PLA$_2$s do not preclude contributions to the activation process by other effects such as accumulation of hydrolysis products (*54*) or membrane lipid phase separation (*55*).

Previous X-ray crystallographic and fluorescence spectroscopy results have suggested that the BthTX-I dimer interface functions as a molecular hinge permitting "open" and "closed" dimer conformations (*21*). A transition between the open and the closed conformation in the membrane-bound BthTX-I dimer would result in the displacement of all of the lipid molecules in contact with the protein, and such a conformational transition could result in disruption of the lipid bilayer and may be the structural basis of the Ca^{2+}-independent membrane damaging activity of the Lys49-PLA$_2$s (*21*). Indeed, changes in the emission depolarization of the fluorescent membrane probe diphenylhexatriene demonstrate that the acyl chain organization in lipid bilayers is significantly perturbed on exposure to these PLA$_2$ homologues (*18*). We have demonstrated here that a transition from the dimeric to the monomeric form of BthTX-I is induced in solution by reducing the pH from 7.0 to 5.0. Furthermore, the dissociation of the dimeric form of BthTX-I to the monomer coincides with the loss of the Ca^{2+}-independent membrane damaging activity. Although the possibility cannot be excluded that the monomeric form of the protein causes the membrane damaging activity observed at pH 7.0, this would imply an inactivation of this activity in the monomer at pH 5.0. The Asp49-PLA$_2$s present a reduced catalytic activity at this pH; however, an argument based on loss of catalytic function is weakened in the case of BthTX-I, since lipid hydrolysis by this protein is not observed experimentally. A further possibility is that the dimer dissociates after interaction with the lipid membrane. If this is the case, the absence of a lag phase in the marker release experiments indicates a rapid dissociation of the membrane-associated dimer. Furthermore, the chemical cross-linking experiments with BthTX-I in the presence of EYPC:DMPA liposomes at pH 7.0 indicate that the dimer remains intact over the 15 min time course of the experiment. We therefore suggest that the initial event of the Ca^{2+}-independent membrane damaging process involves the dimeric form of BthTX-I.

REFERENCES

1. van Deenen, L. L. M, and de Haas, G. H. (1963) *Biochim. Biophys. Acta 70*, 538−553.
2. Dennis, E. A. (1997) *Trends Biochem. Sci. 22*, 1−2.
3. van den Bosch, H. (1980)*Biochim. Biophys. Acta 604*, 191−246.
4. Gutiérrez, J. M., and Cerdas, L. (1984) *Rev. Biol. Trop. 32*, 213−222.
5. Verheij, H. M., Volweerk, J. J., Jansen, E. H., Dijkstra, B. W., and de Haas, G. H. (1980) *Biochemistry 19*, 743−750.
6. Scott, D. L., Otwinowski, Z., Gelb, M. H., and Sigler, P. B. (1990) *Science 250*, 1563−1566.
7. Li, Y., Yu, B. Z., Zhu, H., Jain, M. K., and Tsai, M. D. (1994) *Biochemistry 33*, 14714−14722.
8. van den Bergh, C. J., Slotboom, A. J., Verheij, H. M., and de Haas, G. H. (1989) *J. Cell. Biochem. 39*, 379−390.
9. Gutiérrez, J. M., and Lomonte, B. (1995) *Toxicon 33*, 1405−1424.
10. Holland, D. R., Calncy, L. L., Muchnore, S. W., Rydel, T. J., Einspahr, H. M., Finzel, B. C., Heinrickson, R. L., and Watenpangh, K. D. (1990) *J. Biol. Chem. 265*, 17649−17656.
11. Scott, D. L., Achari, A., Vidal, J. C., and Singler, P. B. (1992) *J. Biol. Chem. 267*, 22645−22657.
12. Arni, R. K., Ward, R. J., Cintra A. C. O., and Giglio, J. R. (1995) *Toxicon 33*, 383−386.
13. Scott, D. L., Mandel A. M., Sigler, P. B., and Honig B. (1994) *Biophys. J. 67*, 493−504.
14. Arni, R. K., and Ward, R. J. (1996) *Toxicon 34*, 827−841.
15. de Azevedo, W. F., Jr., Ward, R. J., Gutiérrez, J. M., and Arni, R. K. (1999) *Toxicon 37*, 371−384.
16. Lee, W., da Silva Giotto, M. T., Marangoni, S., Toyama, M. H., Polikarpov, I., and Garratt, R. C. (2001) *Biochemistry 40*, 28−36.
17. Díaz, C., Gutiérrez, J. M., Lomonte, B., and Gene, J. A. (1991) *Biochim. Biophys. Acta 1070*, 455−460.
18. Rufini, S., Cesaroni, P., Desideri, R. F., Gubensek, F., Gutiérrez, J. M., Luly, P., Maassoud, R., Morero, R., and Pedersen, J. Z. (1992) *Biochemistry 31*, 12424−12430.
19. Pedersen, J. Z., Arcuri, B. F., Moreno, R. D., and Rufini, S. (1994) *Biochim. Biophys. Acta 1190*, 177−180.
20. Homsi-Brandenburgo, M. I., Queiroz, L. S., Santo-Neto, H., Rodrigues-Simoni, L., and Giglio, J. R. (1988) *Toxicon 26*, 615−627.
21. da Silva Giotto, M. T., Garratt, R. C., Oliva, G., Mascarenhas, Y. P., Giglio, J. R., Cintra, A. C. O., de Azevedo, W. F., Jr., Arni, R. K., and Ward, R. J. (1998) *Proteins: Struct., Funct., Genet. 30*, 442−454.
22. Ward, R. J., Monesi, N., Arni, R. K., Larson, R. E., and Paçó-Larson, M. L. (1995) *Gene 156*, 305−306.
23. Laemmli, U. K. (1970) *Nature 227*, 680−685.
24. Szoka, F., and Papahadjopoulos, D. (1978) *Proc. Natl. Acad. Sci. U.S.A. 75*, 4194−4198.
25. Barlett, G. R. (1959) *J. Biol. Chem. 234*, 466−468.
26. Lehrer, S. S. (1971) *Biochemistry 10*, 3254−3263.
27. Anufrieva, E. V., and Gotlib, Yu. Ya (1981) *Adv. Polym. Sci. 40*, 1−68.
28. Semisotnov, G. V., Zikherman, K. Kh., Kasatkin, S. B., Ptitsyn, O. B., and Anufrieva, E. V. (1981) *Bioplymers 20*, 2287−2309.
29. Kulinsky, T., Wennerberg, A. B., Rigler, R., Provencher, S. W., Pooga, M., Langel, U., and Bartfai, T. (1997) *Eur. Biophys. J. 26*, 145−154.
30. Hazlett, T. L., Moore, K. J., Lowe, P. N., Jameson, D. M., and Eccleston, J. F. (1993) *Biochemistry 32*, 13575−13583.
31. Steiner, R. F. (1991) in *Topics in Fluorescence Spectroscopy* (Lakowicz, J. R., Ed.) Vol. 2, pp 1−52, Plenum Press, New York and London.
32. Weber, G., and Shinitzky, M. (1970) *Proc. Natl. Acad. Sci. U.S.A. 65*, 823−830.
33. Helms, M. K., Hazlett, T. L., Mizugushi, H., Hasemann, C. A., Uyeda, K., and Jameon, D. M. (1998) *Biochemistry 37*, 14057−14064.
34. Tcherkasskaya, O., Ptitsyn, O. B., and Knutson, J. R. (2000) *Biochemistry 39*, 1879−1889.

35. Tcherkasskaya, O., Knutson, J. R., Bowley, S. A., Frank, M. K., and Gronenbom, A. M. (2000) *Biochemistry 39*, 11216−11226.
36. Bialik, C. N., Wolf, B., Rachofsky, E. L., Ross, J. B. A., and Laws, W. R. (1998) *Biophys. J. 75*, 2564−2573.
37. Vicent, M., Li De La Sierra, M. I., Berberan-Santos, M. N., Diaz, A., Padron, G., and Gallay, J. (1992) *Eur. J. Biochem. 210*, 953−961.
38. Canduri, F., Mancuso, L. C., Soares, A. M., Giglio, J. R., Ward, R. J., and Arni, R. K. (1998) *Toxicon 36*, 547−551.
39. de Azevedo, W. F., Ward, R. J., Lombardi, F. R., Giglio, J. R., Soares, A. M., Fontes, M. R. M., and Arni, R. K. (1997) *Protein Pept. Lett. 4*, 329−334.
40. Arni, R. K., Fontes, M. R. M., Barberato, J. M., Gutiérrez, J. M., Díaz, C., and Ward, R. J. (1999) *Arch. Biochem. Biophys. 2*, 177−182.
41. Han, S. K., Yoon, E. T., Scott, D. L., Sigler, P. B., and Cho, W. (1987) *J. Biol. Chem. 272*, 3573−3582.
42. Ward, R. J., de Azevedo, W. F., Jr., and Arni, R. K. (1998) *Toxicon 36*, 1623−1633.
43. Demchenko, A. P., and Ladokhin, A. S. (1988) *Biochim. Biophys. Acta 955*, 352−360.
44. Wasylewski, Z., Koloczeck, H., Wasniowska, A., and Slizowska, K. (1992) *Eur. J. Biochem. 206*, 235−242.
45. Myatt, E. A., Stevens, F. J., and Singler, P. B. (1991) *J. Biol. Chem. 266*, 16331−5.
46. Bukowski, T., and Teller, D. C. (1986) *Biochemistry 25*, 8024−8033.
47. Shen, B. W. T., Tsao, F. H., Law, J. H., and Kezdy, F. J. (1975) *J. Am. Chem. Soc. 97*, 1205−1208
48. Wells, M. A. (1971) *Biochemistry 10*, 4074−4078.
49. Wells, M. A. (1973) *Biochemistry 12*, 1086−1093.
50. Smith, C. M., and Wells, M. A. (1981) *Biochim. Biophys. Acta 663*, 687−694.
51. Brunie S., Bolin, J., Gerwith, D., and Singler, P. B. (1985) *J. Biol. Chem. 260*, 9742−9749.
52. Bell, J. D., and Biltonen, R. L. (1989) *J. Biol. Chem. 264*, 12194−12200.
53. Bell, J. D., and Biltonen, R. L. (1992) *J. Biol. Chem. 267*, 11046−11056.
54. Burack, W. R., Dibble, A. R. G., Allietta, M. M., and Biltonen, R. L. (1997) *Biochemistry 36*, 10551−10557.
55. Gadd, M. E., and Biltonen, R. L. (2000) *Biochemistry 39*, 9623−9631.

BI0026728